Fuzzy Approach to Grade Gliomas using Susceptibility-Weighted Images. A Preliminary Study

Francesc Xavier Aymerich
MRI Unit (IDI) / Dept. of Automatic Control
Vall d'Hebron Hospital / UPC
Barcelona, Spain
xavier.aymerich@idi.gencat.cat

Cristina Auger
MRI Unit (IDI)
Vall d'Hebron Hospital
Barcelona, Spain
cristina.auger@idi.gencat.cat

Julio García
MRI Unit (IDI)
Vall d'Hebron Hospital
Barcelona, Spain
juliganu_85@hotmail.com

Elena Martínez-Sáez
Pathology Department
Vall d'Hebron Hospital
Barcelona, Spain
eamartinez@vhebron.net

Francisco Martínez-Ricarte
Neurosurgery Department
Vall d'Hebron Hospital
Barcelona, Spain
fran@neurotrauma.net

Juan Francisco Corral
MRI Unit (IDI)
Vall d'Hebron Hospital
Barcelona, Spain
juanfra.corral@idi.gencat.cat

Alex Rovira
MRI Unit (IDI)
Vall d'Hebron Hospital
Barcelona, Spain
alex.rovira@idi.gencat.cat

***Abstract*—This paper describes a method to grade gliomas examined by magnetic resonance imaging. It is a preliminary study focused only on the features extracted from susceptibility-weighted images. The proposed method involves fusion of classifiers based on decision trees designed using fuzzy techniques. The favorable results indicate that the fuzzy approach may be of particular value for grading gliomas.**

Keywords: brain tumors, classifier fusion, fuzzy classification, fuzzy decision trees, magnetic resonance imaging

I. Introduction

Gliomas are the most common brain tumors, accounting for 70% of primary malignant brain tumors in adults [1]. The World Health Organization (WHO) categorizes gliomas into grades I to IV, with grade I being the least and grade IV the most malignant [2]. The glioma grade is the most important prognostic factor for the patient. Low-grade tumors (I and II) may be amenable to surgery, whereas high-grade tumors must be managed with surgery plus radiochemotherapy and are associated with very low survival rates. Magnetic resonance imaging (MRI) is the initial imaging modality of choice for patients with suspected glioma, and it has a major role in the initial differential diagnosis. However, currently, imaging features are not taken into consideration in the confirmatory diagnosis or grading of glioma, which are solely based on the findings from invasive biopsies [3].

Susceptibility weighted imaging (SWI) is a 3D gradient-recalled echo sequence designed to utilize the susceptibility difference between the deoxygenated blood in veins and the surrounding brain parenchyma to provide a high degree of contrast [4].

SWI has been applied to objectively grade brain tumors, although the methods used for this purpose vary considerably between studies. Park et al. [5] developed a semiquantitative method for grading cerebral neoplasms using intratumoral susceptibility signals (ITSSs), which are hypointense dot-like or linear structures. The grade is determined by the number of ITSS structures depicted within the tumor. However, ITTS detection is not as well suited for low-grade gliomas as for higher-grade gliomas [5][6], and the level of hypointensity varies between the different tumor types. More importantly, identification of an ITSS is a subjective task based on the criteria of the neuroradiologist. Another approach has been proposed by Hori et al. [7], who designed a scheme in which the hypointensity ratio in the SW image relative to the size of the tumor is used to grade brain tumors. Although hypointensity ratios closely correlate with the WHO grading scale of brain tumors, the hypointensity ratio is a semiquantitative method that is ultimately limited by the subjectivity of intra- and interobserver discrepancies in score assignment [2].

Di Ieva et al. [2] have proposed a promising approach, in which a fractal-based method is applied to SWI analysis as an alternative glioma grading method. It was initially developed for 7-T MRI systems, but it has been validated for 3-T systems [8], a field strength commonly used in clinical practice. This method quantifies the geometric complexity of SWI patterns within the tumor resulting from intratumoral microbleeds and neoplastic vasculature by means of their fractal dimension value, used as a morphometric imaging marker to distinguish between low- and high-grade gliomas.

In this paper, we present a fuzzy approach to deal with the inherent vagueness of the information related to intratumoral hypointensity in SWI, with the aim of classifying tumors by grade. The proposed classifier is based on the fusion of decision trees designed using fuzzy techniques. The introduction of fuzzy logic in decision tree design attempts to take advantage of the capability of fuzzy techniques for adapting to and handling problems [9], and their usefulness for classification purposes when the number of cases is small [10]. To our knowledge, this is the first attempt to address glioma grading using fuzzy logic.

The paper is structured as follows: Section II describes the characteristics of the data and MRI sequences used in the study. The next section gives an overview of the proposed algorithm. In section IV, we show some results, and the last section is devoted to presenting the conclusions of the work.

II. Materials

This retrospective study included 44 untreated patients (14 women, 30 men; mean age, 54.41 years; age interval, [18, 78] years) who were diagnosed with glioma on pathological findings and underwent diagnostic preoperative MRI. The histopathological samples obtained by biopsy were classified as grade-II (8 cases), grade-III (7), and grade-IV (29) gliomas.

All MRI scans were performed on a Siemens 3-T Magnetom scanner (Siemens, Erlangen, Germany). The sequences used in this study included post-contrast T2 fluid-attenuated inversion recovery (T2-FLAIR) (repetition time [TR] 9000 ms, echo time [TE] 68 ms, inversion time [TI] 2500 ms, matrix 320x320, field-of-view 220 mm, thickness 4 mm, gap 1.2 mm, acquisition time 3 min 36 s, 25 slices), and SWI (TR 32 ms, TE 24.6 ms, matrix 320x320, field-of-view 250 mm, thickness 3 mm, gap 0 mm, acquisition time 4 min 08 s, 52 slices),

III. Methods

The algorithm proposed for classifying tumors consisted of four stages: segmentation of the region of interest, feature extraction, the fuzzy classifier, and defuzzification. The following subsections describe these stages. The proposed algorithm was designed and tested using Octave 4.0.0 [11].

A. Segmentation of the regions of interest

The first stage consisted of segmenting the tumor in the T2-FLAIR slice where it was best visualized in order to facilitate extraction of the features in the next stage.

A spatial transformation, T, was first applied to the T2-FLAIR images to coregister this volume to the SWI volume. Then, images $I'_{T2-FLAIR}$ were obtained according to:

$$I'_{T2-FLAIR} = T(I_{T2-FLAIR}) \quad (1)$$

where $I_{T2-FLAIR}$ were the original T2-FLAIR images acquired. Coregistration was carried out with the Jim v 6.0 image registration toolkit (Xinapse Systems Ltd, Essex, UK) considering mutual information as cost function and sinc interpolation.

A neuroradiologist selected the slice in $I'_{T2-FLAIR}$ that enabled best visualization of the tumor. Then, using the Jim v 6.0 region of interest (ROI) delineation tool, two regions were manually delineated by a single neuroradiologist: the entire tumor in the slice and the cystic region (Fig. 1). In the analysis, two regions were considered: 1) the whole tumor, and 2) the solid region, defined as the region within the whole tumor complementary to the cystic region.

B. Feature extraction

Thirty-seven features were considered in the image analysis. These features were related to the gray-level, texture, and size properties within the regions of interest defined. These features were the following;

- $p10_l$: 10th percentile of the gray level within the ROI
- $p25_l$: 25th percentile of the gray level within the ROI
- $p50_l$: 50th percentile of the gray level within the ROI
- $p75_l$: 75th percentile of the gray level within the ROI
- $p90_l$: 90th percentile of the gray level within the ROI
- sd_l: standard deviation of the gray level within the ROI
- H_l: entropy within the ROI defined as:

$$H_l = -\sum_{i=0}^{4095} P(i) \log_2 P(i) \quad (2)$$

where $P(i)$ is the probability of gray level i for pixels within the ROI.

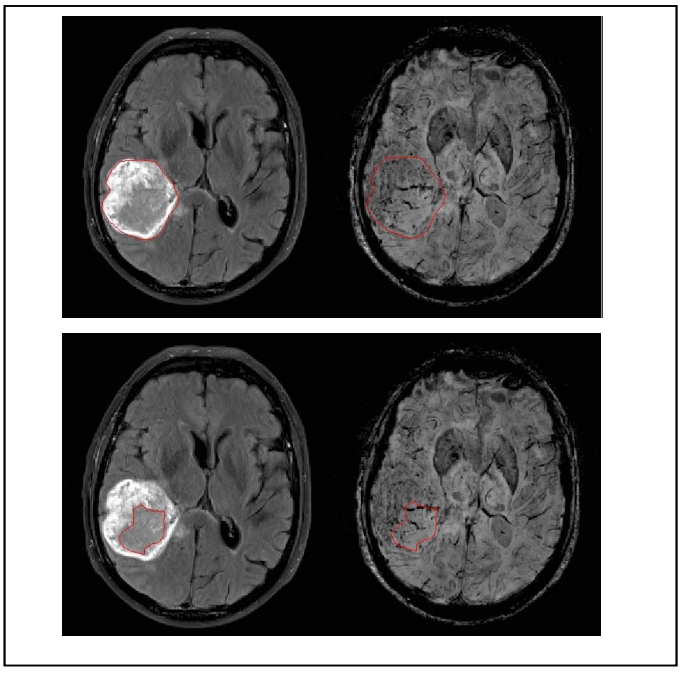

Fig. 1. Example of delineation of the regions of interest, with the delineated contour in red. Images on the left show the post-contrast T2-FLAIR slice where the entire tumor (top) and cystic region (bottom) were delineated. Images on the right show the SWI images where the features within the delineated regions were extracted.

- E_l: Energy within the ROI defined as:

$$E_l = \sum_{i=0}^{4095} P^2(i) \quad (3)$$

where $P(i)$ is the probability of gray level i for pixels within the ROI

- A_l: Area of the ROI
- $npld200_l$: Number of pixels within the ROI with dark-line detection greater than level 200
- $npld250_l$: Number of pixels within the ROI with dark-line detection greater than level 250
- $npld300_l$: Number of pixels within the ROI with dark-line detection greater than level 300
- $nplp500_l$: Number of pixels within the ROI with Laplacian operator greater than level 500
- $nplp600_l$: Number of pixels within the ROI with Laplacian operator greater than level 600
- $nplp700_l$: Number of pixels within the ROI with Laplacian operator greater than level 700
- $npb25_l$: Number of pixels within the ROI with dark-blob detection greater than level 25
- $npb35_l$: Number of pixels within the ROI with dark-blob detection greater than level 35
- $npb50_l$: Number of pixels within the ROI with dark-blob detection greater than level 50

and where l indicates the ROI (*all* when it refers to the whole tumor and *s* when it refers to the solid region).

These features were evaluated for both regions of interest, the whole tumor and the solid region. In addition, the percentage of whole tumor corresponding to the solid region was also considered for the solid region.

The line detection, Laplacian, and blob detection operators were evaluated after transforming the SWI images according to:

$$I'_{SWI}(i,j) = 4095 - I_{SWI}(i,j) \quad (4)$$

in order to detect dark regions within the ROIs.

Line detection was carried out by applying the four 3x3 line detection kernels that responded maximally to horizontal, vertical, and oblique (+45º and -45º) single-pixel-wide lines (Fig. 2a). The line detection value was obtained as the maximum value of the convolution within the ROIs of these four kernels.

The Laplacian operator was applied by using the 5x5 kernel shown in Fig. 2b to carry out the convolution within the ROIs.

Blob detection was performed using gray-level morphological operators in two steps. In the first step, the morphological top-hat operator, using a circular structuring element of radius 4 pixels, was applied to isolate dark structures smaller than this size. The second step consisted in applying a morphological opening using a circular structuring element of radius 1 pixel to remove very thin structures.

Given the small size of the data set, we decided to partition it into subsets following a strategy similar to stratified k-fold cross-validation. In addition, feature extraction was based on application of decision trees to the data set to facilitate interpretability of the variables extracted.

Our data set was then partitioned into 5 non-disjoint subsets, each composed of a 27-case training set and a 6-case test set. Subsets were defined preserving the percentages of grades in the data set. Feature extraction was then was carried out on the 5 training sets to obtain 5 sets of features.

Features were extracted from each subset of the training set using learning based on the RapidMiner 7.2 decision tree module [12]. This module is an implementation of Quinlan's C4.5 algorithm [13], in which we chose the parameters after applying a heuristic analysis. The parameters selected were the following:

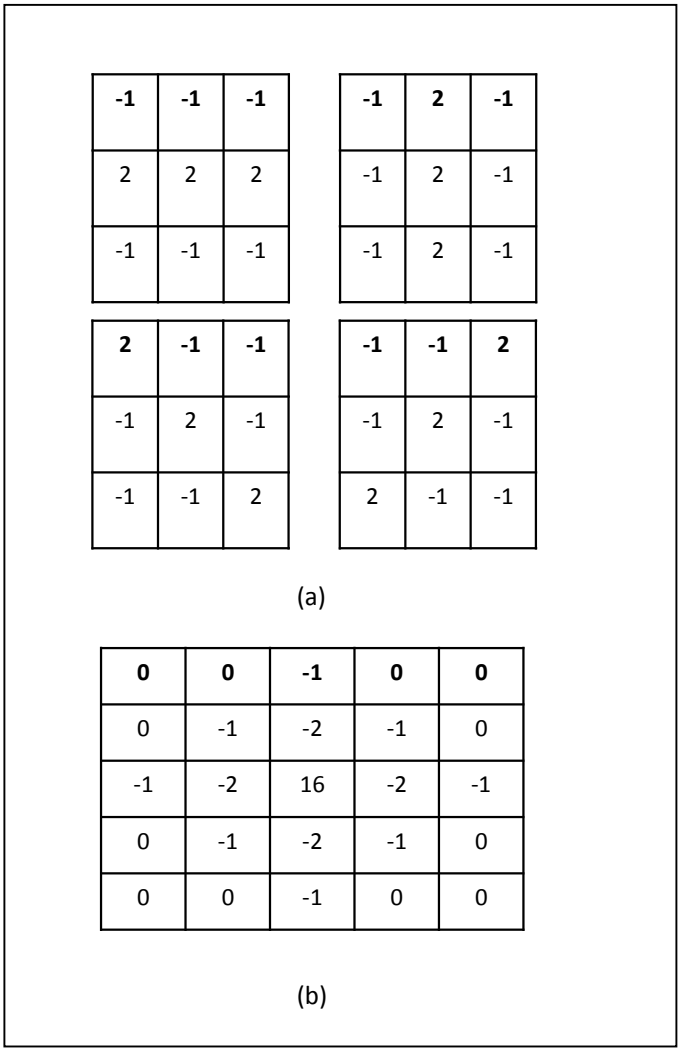

Fig. 2. Kernels used in (a) line detection, and (b) to apply the Laplacian operator

- Criterion: gain ratio
- Maximal depth: 5
- Pruning: yes
- Confidence: 0.25
- Prepruning: yes
- Minimal gain: 0.1
- Minimal leaf size: 1
- Minimal size for split: 4
- Number of prepruning alternatives: 3

Application of this algorithm to each subset allowed us to extract:

- A decision tree based on three or four features
- The crisp thresholds for this decision tree
- The classification of each case according to the thresholds and the decision tree

An example of the decision trees obtained and their respective thresholds for a subset of the training set are shown in Fig. 3. By applying this strategy to each subset, we obtained 5 decision trees, one for each subset.

The extracted features were denoted as a_{mn}, where m was the index of the feature, and n the index of the subset of the training set.

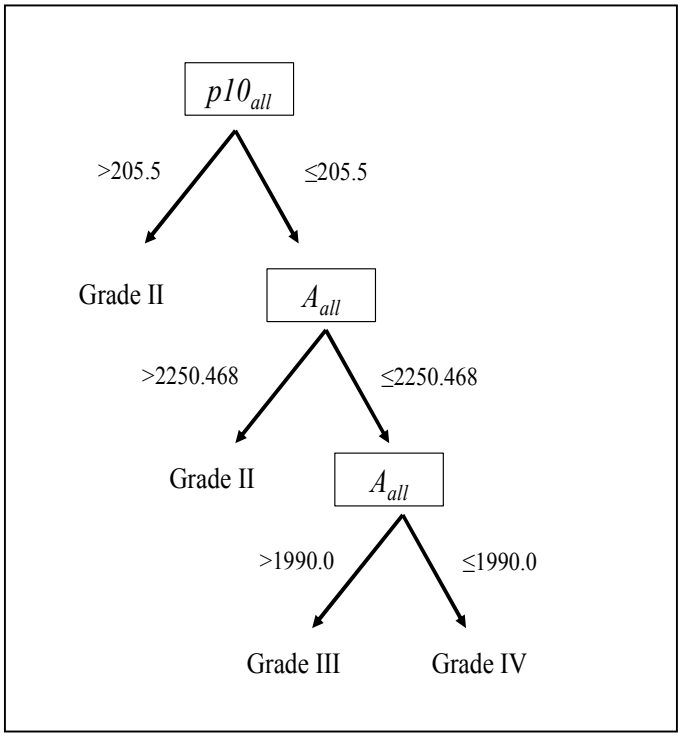

Fig. 3. Example of the decision trees obtained using the decision tree module from the RapidMiner software

C. Fuzzy classifier

To design the classifier, we considered the architecture of the crisp decision trees obtained for each subset of the training set. We then fuzzified the crisp decision trees, defining the membership functions that characterized the low and high behavior of the feature corresponding to each tree node with regard to its threshold. Classifier fusion was then carried out by combining the classifiers based on the fuzzy decision trees, assuming that all decision trees had the same weight in the classification of a case. The proposed classifier involved two levels of classification and a final defuzzification step. The first level consisted in definition of the fuzzy sets, related to the extracted features, and the aggregation rules to fuzzify the crisp decision trees obtained for each subset. The second level consisted in fusion of these fuzzy classifiers. Finally, the classification was obtained by defuzzifying the resulting fuzzy set. The following subsections describe all these steps.

1) Definition of fuzzy sets: For each feature a_{mn} the fuzzy sets associated with values that were lower $F_{l,a_{mn}}$ and higher $F_{h,a_{mn}}$ than the threshold th_{mn} were characterized by their membership functions $\mu_{l,a_{mn}}$ and $\mu_{h,a_{mn}}$, which were obtained according to the following definitions:

Definition 1. The membership function $\mu_{\mathrm{l,a_{mn}}}$ that defined the fuzzy set associated with a_{mn} values that were lower than th_{mn}, $\mathrm{F_{l,a_{mn}}}$, is given by

$$\mu_{\mathrm{l,a_{mn}}}(x) = \begin{cases} 1, & x < 0.8th_{mn} \\ 1 - 0.5\frac{x-0.8th_{mn}}{0.2th_{mn}}, & 0.8th_{mn} \le x < 1.2th_{mn} \\ 0, & x \ge 1.2th_{mn} \end{cases} \quad (5)$$

Definition 2. The membership function $\mu_{\mathrm{h,a_{mn}}}$ that defined the fuzzy set associated with a_{mn} values that were higher than th_{mn}, $\mathrm{F_{h,a_{mn}}}$, is given by

$$\mu_{\mathrm{h,a_{mn}}}(x) = \begin{cases} 1, & x \ge 1.2th_{mn} \\ 1 + 0.5\frac{x-1.2th_{mn}}{0.2th_{mn}}, & 0.8th_{mn} \le x < 1.2th_{mn} \\ 0, & x < 0.8th_{mn} \end{cases} \quad (6)$$

2) Aggregation of fuzzy sets: In this step, we aggregated the fuzzy sets $F_{l,a_{mn}}$ and $F_{h,a_{mn}}$ associated with each feature a_{mn} to classify each case into one of three grades. To do so, we defined new fuzzy sets named F_{IIn}, F_{IIIn}, and F_{IVn}, associated with the three grades, II, III, and IV, considering the features of the subset n of the training set. A classifier could thus be associated with the fuzzy decision tree obtained from the subset n and its output could be defined as follows:

Definition 3. The output of the nth classifier is $D_n(x) = (\mu_{IIn}(x), \mu_{IIIn}(x), \mu_{IVn}(x))$, for $1 \le n \le 5$, where μ_{IIn}, μ_{IIIn}, and μ_{IVn} are the membership functions associated with the fuzzy sets F_{IIn}, F_{IIIn}, and F_{IVn} and obtained by aggregation of $\mu_{l,a_{mn}}$ and $\mu_{h,a_{mn}}$ based on the aggregation rules derived from the architecture of the corresponding decision tree.

Given that the first level in the classification consisted of 5 classifiers, we obtained a set of classifiers $D=\{D_1, D_2, \ldots, D_5\}$ whose outputs were determined according to Definition 3, and whose decision profile was defined as follows:

Definition 4. The decision profile of *D*, *DP(x)*, is given by

$$DP(x) = \begin{pmatrix} \mu_{II1}(x) & \mu_{III1}(x) & \mu_{IV1}(x) \\ & \dots & \\ \mu_{IIn}(x) & \mu_{IIIn}(x) & \mu_{IVn}(x) \\ & \dots & \\ \mu_{II5}(x) & \mu_{III5}(x) & \mu_{IV5}(x) \end{pmatrix} \quad (7)$$

where $\mu_{IIn}(x)$, $\mu_{IIIn}(x)$, and $\mu_{IVn}(x)$, for $1 \le n \le 5$, are the membership functions associated with the fuzzy sets F_{IIn}, $F_{IIIn,}$ and F_{IVn} of $D_n(x)$,determined according to Definition 3.

3) Fusion of classifiers: In this step, we merged the outputs obtained in the previous step to obtain a new classifier, $\widehat{D}$.

To do so, we defined three fuzzy sets, F_{II}, F_{III}, and F_{IV} associated with the three grades, *II*, *III,* and *IV*, which are characterized by the membership functions μ_{II}, μ_{III}, and μ_{IV} respectively. The output of the classifier was then defined as follows:

Definition 5. The output of the classifier $\widehat{D}(x)$ is given by

$$\widehat{D}(x) = \left(\mu_{II}(x), \mu_{III}(x), \mu_{IV}(x)\right) = R(DP(x)) \quad (8)$$

where *R* is an aggregation rule.

The aggregation rule *R* was implemented by applying ordered weighted averaging (OWA) operators [14]. An OWA operator can be defined as follows:

Definition 6. An OWA operator of dimension n is a mapping $f: R^n \to R$ that has an associated n vector $w = (w_1, w_2, \dots, w_n)^T$ such that

$$w_i \in [0,1],\ 1 \le i \le n$$

Furthermore,

$$f(a_1, a_2, \dots, a_n) = w \cdot b = \sum_{j=1}^{n} w_j b_j \quad (9)$$

where $w{\cdot}b$ is the dot product of *w* and *b*, being $b = (b_1, b_2, \dots, b_n)^T$ a permuting of $a = (a_1, a_2, \dots, a_n)^T$ so that b_j is the *j*th largest element of *a*.

Then, the aggregation rule applied to the decision profile *DP(x)*, *R(DP(x))*, was defined as follows:

Definition 7. The aggregation rule applied to the decision profile *DP(x)*, *R(DP(x))*, is given by

$$R\left(DP(x)\right) = w \cdot P(x) = w \cdot \begin{pmatrix} p_{II1}(x) & p_{III1}(x) & p_{IV1}(x) \\ & \dots & \\ p_{IIi}(x) & p_{IIIi}(x) & p_{IVi}(x) \\ & \dots & \\ p_{II5}(x) & p_{III5}(x) & p_{IV5}(x) \end{pmatrix} \quad (10)$$

where *P(x)* is the permuting of *DP(x)* whose vectors $(p_{Y1}(x), \dots, p_{Yi}(x), \dots, p_{Y5}(x))^T$ for $Y \in \{II, III, IV\}$ were obtained by permuting the vectors $V_Y = (\mu_{Y1}(x), \dots, \mu_{Yi}(x), \dots, \mu_{Y5}(x))^T$ so that $p_{Yi}(x)$ is the *i*th largest element of V_Y. And the weighting vector, *w*, was determined by heuristic analysis of the outputs for the training set.

4) Defuzzification: Finally, the defuzzification stage allowed each case to be classified into one of the three grades initially considered: *II*, *III,* or *IV*. This process was based on selection of the grade with the highest membership degree in $\widehat{D}(x)$ $(max\left(\widehat{D}(x)\right))$.

A diagram of the overall proposed classifier applied to a case *x* is shown in Fig. 4. This diagram includes the 5 classifiers based on fuzzy decision trees, their outputs, $D_n(x)$ $(1 \le n \le 5)$, the fusion step based on OWA aggregation operators, with which $\widehat{D}(x)$ is obtained, and selection of the grade by application of the maximum operator.

IV. Results

To obtain the results, the data set was divided in two subsets. The first subset, consisting of 33 cases, was focused on the design of the algorithm, and the second subset, consisting of 11 cases, was used for validation purposes. Evaluation of the results was carried out using the accuracy quality index, defined as follows:

Definition 8. The accuracy in classification of a multi-class problem is given by

$$Acc = \frac{\sum_{i=1}^{n} c_{ii}}{\sum_{i=1}^{n}\sum_{j=1}^{n} c_{ij}} \quad (11)$$

where c_{ij} is the element corresponding to row *i* and column *j* of the confusion matrix, c_{ii} is an element of the diagonal of the confusion matrix, and *n* is the dimension of the *n x n* confusion matrix.

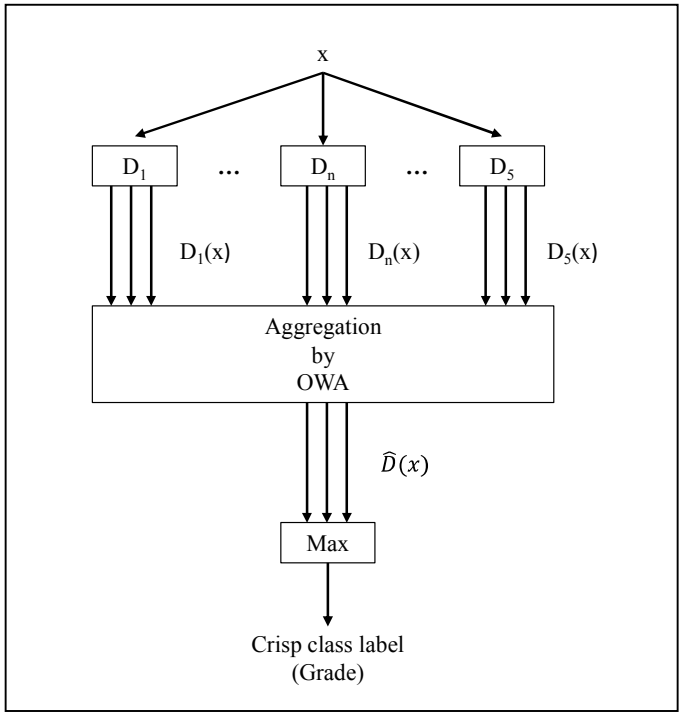

Fig. 4. Diagram of the proposed classifier

Given that we proposed a two-level classifier, we evaluated the results for each of the two levels separately. First, we considered only the decision tree classifiers designed from the extracted features; then, we added the fuzzification step and fusion of the fuzzy classifiers. Finally, we considered the validation step, applying the proposed fuzzy classifier to the validation subset of the data.

A. Classifiers resulting from feature extraction

The feature extraction process yielded the following features involved in the classification: $p10_{all}$, A_{all}, $p10_s$, A_s, and $npb25_{all}$. Using these features, the *decision tree module* of RapidMiner *7.2* enabled definition of five decision trees to implement each of the five classifiers from the first stage.

The mean accuracy of this first level of the classifier, considering 5-fold cross-validation, was 0.62, with interval values [0.43, 0.83].

B. Fuzzification and fusion of classifiers

Each of the decision trees obtained in the previous stage was fuzzified according to the procedure described in section *III C*, and then fused using a majority vote schema. To implement this schema, we considered the following vector within the OWA operator:

$$w = (0, 0, 1, 0, 0)^T \tag{12}$$

The mean accuracy after this fusion level of the classifier considering 5-fold cross-validation was 0.90 with interval values [0.83, 1.0], a clear improvement over the accuracy obtained in the first stage.

C. Validation

In a final stage, the proposed classifier was validated using a subset of the data set including 11 cases (2 grade II, 1 grade III, and 8 grade IV). Cases in this subset were not involved in the design of the proposed classifier.

The accuracy obtained in this validation stage was 0.64.

D. Comparison with the crisp approach

In order to study the advantage of introducing the fuzzy approach, a crisp version of the proposed classifier was also considered. This version excluded the fuzzification step and used the OWA operator to combine crisp outputs.

The mean accuracy after the fusion level of the classifier considering 5-fold cross-validation was 0.87 with interval values [0.67, 1.0]. The classifier was also tested using the 11 cases involved in the validation stage, and an accuracy of 0.54 was obtained.

V. Conclusions

In this paper, we present a fuzzy algorithm to grade gliomas. In this preliminary study, we only considered features visualized in SW images for the classification, and the classifier was focused only on grades II to IV of the WHO classification. Although the number of cases is limited, the results show that the tumor-related information in SW images is useful for grading, and the fuzzy approach is an interesting method to deal with this type of classification problem. The results also show that introduction of the fusion stage is the main reason for the gain introduced by the fuzzy approach. The increase of accuracy observed in the fuzzy version of the classifier in relation to the crisp version suggests the value of the fuzzy approach for tumor grading. However, the introduction of complementary information, such as features from perfusion and/or diffusion MRI sequences could improve the results, and this is the aim of future work in this line.

Acknowledgment

The authors thank Celine Cavallo for English language support.

References

[1] K. E. Emblem, D. Schele, P. Due-Tonnessen, B. Nedregaard, T. Nome, J.K. Hald et al., "Histogram analysis of MR imaging-derived cerebral blood volume maps: combined glioma grading and identification of low-gradeoligodendroglial subtypes", AJNR Am J Neuroradiol, vol. 29, pp. 1664-1670, 2008.

[2] A. Di Ieva, S. Göd, G. Grabner, F. Grizzi, C. Sherif, C. Matula et al., "Three-dimensional susceptibility-weighted imaging at 7T using fractal-based quantitative analysis to grade gliomas", Neuroradiology, vol. 55, pp. 35-40, 2013.

[3] G.N. Fuller, and B.W. Scheithauer, "The 2007 revised World Health Organization (WHO) classification of tumors of the central nervous system: newly codified entities", Brain Pathol, vol. 17, pp. 304-307, 2007.

[4] J.R. Reichenbach, R. Venkatesan, D.J. Schillinger, D.K. Kido, and E.M. Haacke, "Small vessels in the human brain: MR venography with deoxyhemoglobin as an intrinsic contrast agent", Radiology, vol. 204, pp. 272-277, 1997.

[5] M.J. Park, H.S. Kim, G.H. Jahng, C.W. Ryu, S.M. Park, and S.Y. Kim, "Semiquantitative assessment of intratumoral susceptibility signals using non-contrast-enhanced high-field high-resolution susceptibility-weighted imaging in patients with gliomas: comparison with MR perfusion imaging", AJNR Am J Neuroradiol, vol. 30, pp. 1402-1408, 2009.

[6] S.M. Park, H.S. Kim, G.H. Jahng, G.W. Ryu, and S.Y. Kim, "Combination of high-resolution susceptibility-weighted imaging and the aparent diffusion coefficient: added value to brain tumour imaging and clinical feasibility of non-contrast MRI at 3T", Br J Radiol, vol. 83, pp. 466-475, 2010.

[7] M. Hori, H. Mori, S. Aoki, O. Abe, T. Masumoto, S. Kunimatsu, et al., "Three-dimensional susceptibility weighted imaging at 3T using various image analysis methods in the estimation of grading intracranial gliomas", Magn Reson Imaging, vol. 28, pp.594-598, 2010.

[8] A. Di Ieva, P.J. Le Reste, B. Carsin-Nicol, JC. Ferre, and M.D. Cusimano, "Diagnostic value of fractal analysis for the differentiation of brain tumors using 3-Tesla magnetic resonance susceptibility-weighted imaging", Neurosurgery, vol. 79, pp. 839-845, 2016

[9] C. Olaru, and L. Wehenkel, "A complete fuzzy decision tree technique", Fuzzy Sets and Systems, vol. 138, pp. 221–254, 2003.

[10] L.I. Kuncheva, Fuzzy Classifier Design, Physica-Verlag Heidelberg, New York, 2000.

[11] J.W. Eaton, GNU Octave Manual, Network Theory Limited, 2002.

[12] I. Mierswa, M. Wurst, R. Klinkenberg, M. Scholz, T. Euler, "YALE: rapid prototyping for complex data mining tasks", Proceedings of the 12th ACM SIGKKD International Conference on Knowledge and Data Mining, pp. 935–940, 2006.

[13] J.R. Quinlan, C4.5: Programs for Machine Learning, Morgan Kaufmann Publishers, San Mateo, 1993.

[14] R.R. Yager, "Families of OWA operators", Fuzzy Sets and Systems, vol. 59, pp. 125–148, 1993.